Modeling quasi-static and fatigue-driven delamination migration

Authors: N. V. De Carvalho
J. G. Ratcliffe
B. Y. Chen
S. T. Pinho
P. M. Baiz
T. E. Tay

ABSTRACT

An approach was proposed and assessed for the high-fidelity modeling of progressive damage and failure in composite materials. It combines the Floating Node Method (FNM) and the Virtual Crack Closure Technique (VCCT) to represent multiple interacting failure mechanisms in a mesh-independent fashion. Delamination, matrix cracking, and migration were captured failure and migration criteria based on fracture mechanics. Quasi-static and fatigue loading were modeled within the same overall framework. The methodology proposed was illustrated by simulating the delamination migration test, showing good agreement with the available experimental data.

INTRODUCTION

Damage in composite materials generally occurs as a combination of different and interacting failure mechanisms, e.g. delamination and matrix cracking. Capturing these interactions accurately is essential to confidently model and predict progressive damage and failure. Several approaches have recently been proposed

N. V. De Carvalho, National Institute of Aerospace, 100 Exploration Way, 23666 Hampton, VA, USA.
J. G. Ratcliffe, NASA Langley Research Center, 2 W. Reid St., Hampton, VA 23681, USA.
B. Y. Chen, Department of Mechanical Engineering, National University of Singapore, 9 Engineering Drive 1, 117575 Singapore.
S. T. Pinho, Department of Aeronautics, Imperial College London, SW7 2AZ London, UK.
P. M. Baiz, Department of Aeronautics, Imperial College London, SW7 2AZ London, UK.
T. E. Tay, Department of Mechanical Engineering, National University of Singapore, 9 Engineering Drive 1, 117575 Singapore.

that explicitly model different failure mechanisms and attempt to capture their interaction [1-3]. The present approach combines the Floating Node Method (FNM) [4] with the Virtual Crack Closure Technique (VCCT) [5,6] to explicitly account for different failure mechanisms and their interaction. Delamination, matrix cracking, and migration events are all modeled with the same FNM element using failure and migration criteria based on fracture mechanics. Preliminary results for quasi-static loading using this approach have been presented in [7]. The approach was validated using recent experimental results in which a setup capable of isolating a single complete migration event was developed [8], where migration is defined as the transition of a delamination from its current ply interface to a new interface via transverse ply cracking. In the present paper, some of the results obtained in [7] will be reviewed. In addition, the approach developed in [7] is combined with a fatigue algorithm and a novel migration criterion, and used to simulate delamination migration under fatigue loading conditions.

FLOATING NODE METHOD (FNM)

The FNM is a recently proposed numerical method, capable of representing multiple evolving discontinuities in solids [4]. In the present section, an overview of the method is provided, further details and comparison with other existing methods are given in [4].

Element formulation

The static equilibrium of a body with volume Ω under body forces with density $\mathbf{f}$ (acting on Ω) and traction $\mathbf{t}$ acting on the boundary Γ_Ω can be expressed in the weak form as:

$$\int_\Omega \boldsymbol{\epsilon}^{\mathrm{T}}(\mathbf{v})\boldsymbol{\sigma}(\mathbf{u})\mathrm{d}\Omega = \int_\Omega \mathbf{v}^{\mathrm{T}}\mathbf{f}\mathrm{d}\Omega + \int_{\Gamma_\Omega} \mathbf{v}^{\mathrm{T}}\mathbf{t}\mathrm{d}\Gamma_\Omega \qquad (1)$$

where $\mathbf{u}$ is the displacement vector; $\mathbf{v}$ is the test function; $\boldsymbol{\epsilon}$ is the strain tensor related to $\mathbf{u}$ through the differential operator relative to Cartesian coordinates $\mathcal{L}_\mathbf{x}$ as $\boldsymbol{\epsilon} = \mathcal{L}_\mathbf{x}(\mathbf{u})$; and $\boldsymbol{\sigma}$ is the stress tensor related to the strains through Hooke's law as $\boldsymbol{\sigma} = \mathbf{D}\boldsymbol{\epsilon}$, with $\mathbf{D}$ being the constitutive tensor. In the Floating Node Method, each real node "i" is characterized by its nodal coordinates $\mathbf{x}_i$ and associated Degrees of Freedom (DoF) $\mathbf{q}_i$. In addition, an FNM element contains a suitable number of floating DoF without pre-defined associated nodal position vectors. These additional floating nodes are used to represent discontinuities. Their number varies with the number and type of discontinuities, weak or strong, modeled within each element. A strong discontinuity is defined as a jump in a field quantity (e.g. displacements), while a weak discontinuity is defined as a jump in the gradient of a field quantity (e.g. strains). Figure 1 shows an example of such an element with four nodes and four additional sets of floating DoF required to represent a strong discontinuity.

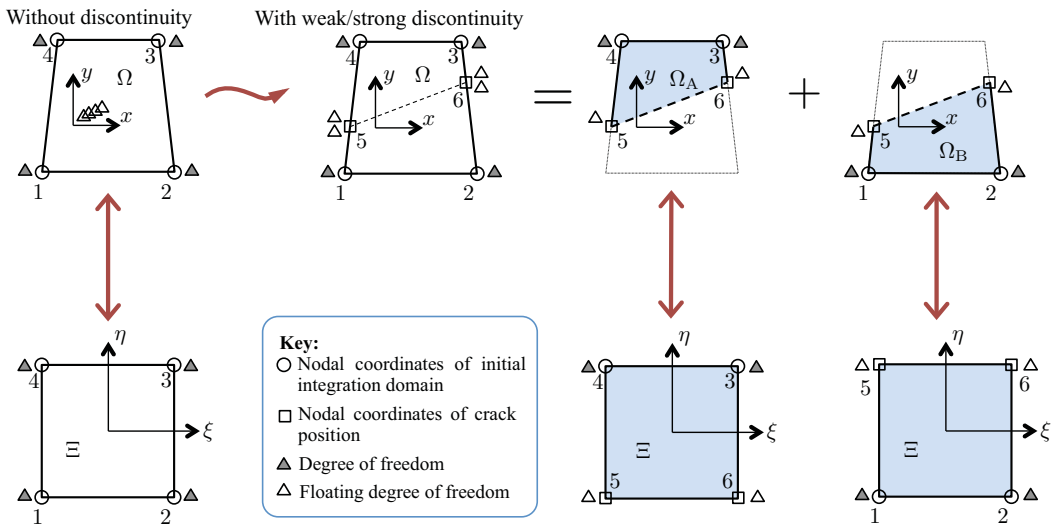

Figure 1. Overview of the Floating Node Method (FNM).

ELEMENT FORMULATION WITH WEAK/STRONG DISCONTINUITY

Once a discontinuity in the element is defined, the element is split in two or more partitions (depending on the discontinuity). Without loss of generality, a case in which the element is split in two partitions, Ω_A and Ω_B, is illustrated in fig. 1. For each partition, Ω_A and Ω_B, a vector of nodal coordinates, $\mathbf{x}_{\Omega_A}$ and $\mathbf{x}_{\Omega_B}$, is defined. For the case in fig. 1:

$$\mathbf{x}_{\Omega_A}^{T} = [\mathbf{x_5}, \mathbf{x_6}, \mathbf{x_3}, \mathbf{x_4}] \tag{2}$$

$$\mathbf{x}_{\Omega_B}^{T} = [\mathbf{x_1}, \mathbf{x_2}, \mathbf{x_6}, \mathbf{x_5}] \tag{3}$$

Each partition has a separate Jacobian:

$$\mathbf{J}_A = \frac{d\mathbf{x}}{d\boldsymbol{\xi}} = \frac{d\mathbf{N}}{d\boldsymbol{\xi}} \mathbf{x}_{\Omega_A} \tag{4}$$

$$\mathbf{J}_B = \frac{d\mathbf{x}}{d\boldsymbol{\xi}} = \frac{d\mathbf{N}}{d\boldsymbol{\xi}} \mathbf{x}_{\Omega_B} \tag{5}$$

The displacements $\mathbf{u}_A$ and $\mathbf{u}_B$, in partitions Ω_A and Ω_B, respectively, are interpolated separately from the DoF $\mathbf{q}_A$ and $\mathbf{q}_B$ associated with each partition:

$$\mathbf{u}_A = \mathbf{N}\mathbf{q}_A \quad \text{and} \quad \mathbf{u}_A = \mathbf{N}\mathbf{q}_A \tag{6}$$

These DoF, $\mathbf{q}_A$ and $\mathbf{q}_B$, did not have an associated position beforehand, and therefore were considered to be "floating". As the discontinuity is defined, they are linked to the respective position vector. In the case of fig. 1, which represents a strong discontinuity, $\mathbf{q}_A^T = [\mathbf{q_5}, \mathbf{q_6}, \mathbf{q_3}, \mathbf{q_4}]$ and $\mathbf{q}_B^T = [\mathbf{q_1}, \mathbf{q_2}, \mathbf{q_{6'}}, \mathbf{q_{5'}}]$. Note that there are four different sets of floating DoF: $\mathbf{q_5}$ is different from $\mathbf{q_{5'}}$ and $\mathbf{q_6}$ is different from $\mathbf{q_{6'}}$. If a weak discontinuity were to be modeled, only two sets of

floating DoF would be included in the element, and the DoF with a prime would coincide with those without a prime.
The strains then become:

$$\boldsymbol{\epsilon}_A = \mathcal{L}_{\mathbf{x}}(\mathbf{u}_A) = \mathcal{L}_{\boldsymbol{\xi}}(\mathbf{N})\mathbf{J}_A{}^{-1}\mathbf{q}_A = \mathbf{B}_A\mathbf{q}_A \tag{7}$$

$$\boldsymbol{\epsilon}_B = \mathcal{L}_{\mathbf{x}}(\mathbf{u}_B) = \mathcal{L}_{\boldsymbol{\xi}}(\mathbf{N})\mathbf{J}_B{}^{-1}\mathbf{q}_B = \mathbf{B}_B\mathbf{q}_B \tag{8}$$

The stiffness matrices for partitions Ω_A and Ω_B are:

$$\mathbf{K}_A = \int_{\Xi} \mathbf{B}_A^T\mathbf{D}\mathbf{B}_A \det(\mathbf{J}_A)\mathrm{d}\Xi \tag{9}$$

$$\mathbf{K}_B = \int_{\Xi} \mathbf{B}_B^T\mathbf{D}\mathbf{B}_B \det(\mathbf{J}_B)\mathrm{d}\Xi \tag{10}$$

and the force vectors:

$$\mathbf{Q_A} = \int_{\Xi} \mathbf{N^T f}\det(\mathbf{J_A})\mathbf{d}\Xi + \int_{\boldsymbol{\Gamma}_{\Xi}} \mathbf{N^T f}\det(\mathbf{J_A})\mathbf{d}\Xi \tag{11}$$

$$\mathbf{Q_B} = \int_{\Xi} \mathbf{N^T f}\det(\mathbf{J_B})\mathbf{d}\Xi + \int_{\boldsymbol{\Gamma}_{\Xi}} \mathbf{N^T f}\det(\mathbf{J_B})\mathbf{d}\Xi \tag{12}$$

Finally, the equations of equilibrium can be written as:

$$\mathbf{K_A q_A} = \mathbf{Q_A} \text{ and } \mathbf{K_B q_B} = \mathbf{Q_B} \tag{13}$$

ELEMENT TOPOLOGY AND ASSEMBLY

To illustrate this approach, a floating node element capable of modeling two weak interfaces with an arbitrary crack between them was implemented, as shown in fig. 2(a). The nodal position of the initial integration domain, and the real and floating DoF are indicated in the figure. Each floating DoF is associated with either an edge or the inner domain of the element. Once weak/strong discontinuities are detected, the floating DoF at the edges are used to determine the solution for the nodal positions created by the intersection of these discontinuities with the element edges (figs. 2(b) to 2(e)). The additional inner floating DoF are used to determine the solution for the nodal positions created by the intersection of multiple cracks within the element (fig. 2(f)). In figs 2(b) to (f), only the floating DoF used are represented. In each case, the floating DoF that are not used have no assigned position, only a topological relation to an edge or to the inner domain. During assembly, inner floating DoF can be removed from the analysis through static condensation. The floating DoF associated with the edges are assembled with the corresponding DoF of neighboring elements, and will therefore have a unique position in the global DoF vector. All floating DoF are then used as required to model weak/strong discontinuities as they evolve throughout the simulation. To

accommodate certain crack geometries while enabling the integration of the domain of interest, the elements may need to be partitioned in triangles rather than rectangles only, figs. 2(d) and 2(f). Nevertheless, also in this case, the general procedure outlined in the previous section is used to integrate these elements, and determine their stiffness.

The approach can be extended to model an arbitrary number of weak and strong discontinuities within an element, and therefore an arbitrary number of plies and interacting cracks, provided its topology, including the number of floating DoF, is adequately defined [4, 7].

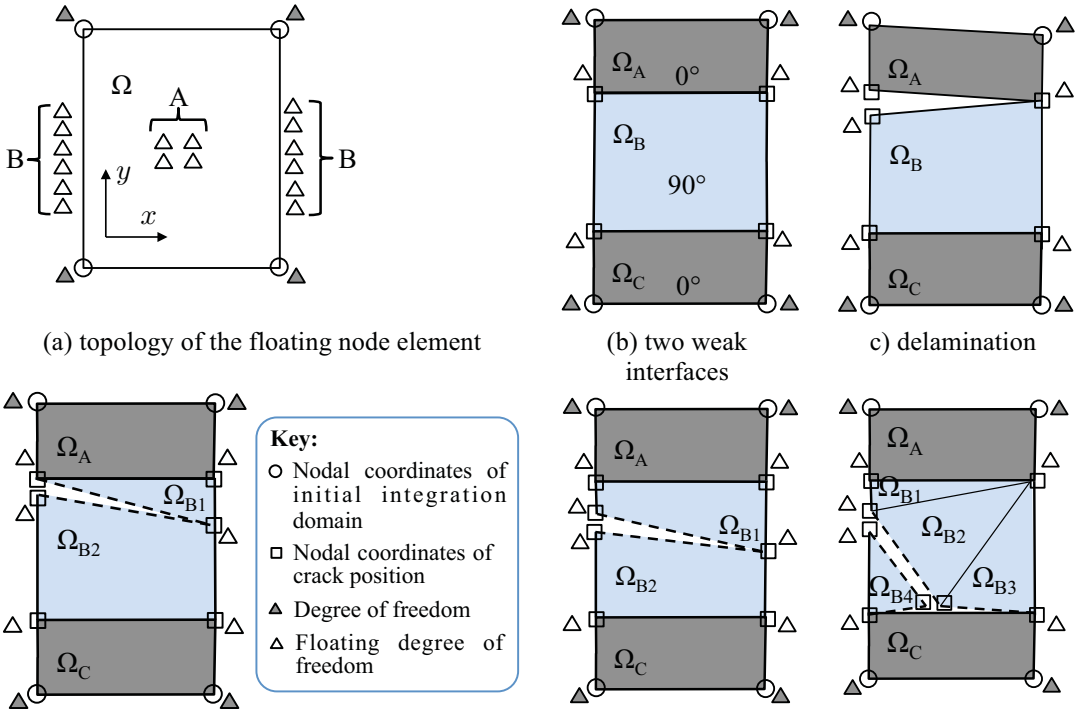

(a) topology of the floating node element

(b) two weak interfaces

c) delamination

d) delamination with migration to matrix crack

e) matrix crack

f) matrix crack migration to delamination

Figure 2. Representation of the floating node element used in the present work, illustrating how the different weak/strong discontinuities scenarios are accommodated.

VIRTUAL CRACK CLOSURE TECHNIQUE (VCCT)

In the present work, the FNM method has been coupled with the Virtual Crack Closure Technique (VCCT) [5]. A comprehensive review of VCCT is provided in [6]. Traditionally, VCCT is used to obtain energy release rates in cases where the crack path is known beforehand and can be aligned with the elements' edges, such as the case for delamination. In VCCT, the Mode I and II energy release rates are obtained from [6]:

$$G_I = \frac{1}{2a_1} F_n [\![q_n]\!] \left(\frac{a_1}{a_2}\right)^{1/2} \tag{14}$$

$$G_{II} = \frac{1}{2a_1} F_t [\![q_t]\!] \left(\frac{a_1}{a_2}\right)^{1/2} \tag{15}$$

where F_n and F_t are the normal and tangential components of internal force vector **F** at the crack tip; $[\![q_n]\!]$ and $[\![q_t]\!]$ are the normal and tangential components of the displacement jump $[\![\mathbf{q}]\!]$ between the nodes immediately behind the crack tip; and a_1 and a_2 are the lengths of the crack in the elements behind and ahead of the crack tip, respectively (fig. 3). When combining VCCT with FNM, the forces and displacements needed to obtain the energy release rates, Eqs (14) and (15), are computed at the floating DoF as the crack develops (fig. 3). Additionally, floating DoF can also be added along a virtual crack plane up to a distance r, named the 'enrichment radius', r_{enr}. The associated floating nodes provide additional degrees of freedom along this path, which enable the accurate modeling of the deformations near the crack tip [4]. At the end of the enrichment radius, the displacements of the floating DoF are interpolated from the displacements of the real DoF. In the present work, the enrichment radius was chosen to be equal to the largest in-plane dimension of the numerical model.

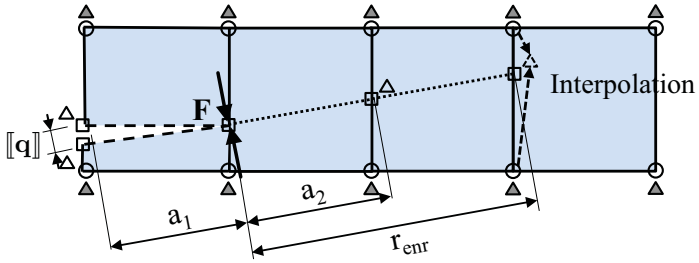

Figure 3. Virtual Crack Closure Technique and Floating Node Method for arbitrary crack propagation.

DELAMINATION PROPAGATION

Quasi-static loading

In this paper, delamination is modeled using VCCT to compute the energy release rates G_I and G_{II} at each delamination front position. These are then used in a failure criterion:

$$f(G_I, G_{II}) = \frac{G_T}{G_c} - 1 = 0 \tag{16}$$

where $G_T = G_I + G_{II}$, and G_c is the critical energy release rate given by [9]:

$$G_c = G_{Ic} + (G_{IIc} - G_{Ic}) \left(\frac{G_{II}}{G_T}\right)^{\eta} \tag{17}$$

For delamination growth according to this criterion, G_c is assumed to equal the critical energy release rate of the interface, G_c^{Int}. The delamination front is advanced by one element along the interface when $G_T = G_c^{Int}$.

Fatigue loading

Under fatigue loading, the delamination growth rate is determined using a Paris Law type relationship:

$$\frac{\mathrm{d}a}{\mathrm{d}N} = A(G_{Tmax})^n \tag{18}$$

where $G_{Tmax} = G_{Imax} + G_{IImax}$. Since delamination is growing under mixed mode conditions, both A and n are assumed to vary with mode mixity. Several expressions have been proposed for characterizing the propagation rate under mixed mode conditions [10]. However, no general expression has yet found widespread acceptance. In the present work, a first order approximation is used to characterize the variation of A and n with mode mixity:

$$A = A_I + (A_{II} - A_I)\left(\frac{G_{IImax}}{G_T}\right) \tag{19}$$

$$n = n_I + (n_{II} - n_I)\left(\frac{G_{IImax}}{G_T}\right) \tag{20}$$

where pairs A_I, n_I, and A_{II}, n_{II} were obtained from fatigue testing under Mode I and Mode II conditions for the material being used, respectively [11, 12]. Recent experiments indicate that a higher order approximation can possibly improve the representation of the variation of A and n with mode mixity [13]. Experimental results also confirm the monotonic behavior assumed in a first order approximation. Therefore, for simplicity, Equations 19 and 20 will be used in this study.

The growth rate obtained from Equation 18 is then used to determine crack propagation using the fatigue algorithm implemented, which is discussed in a subsequent section. Note that Equation 18 does not account for the effects of loading ratio, and frequency. Therefore, its use is currently only recommended to predict the growth rate for R-ratios and frequencies that correspond to those used to generate the delamination fatigue characterization data.

MATRIX CRACK PROPAGATION

Quasi-static loading

In the present study, matrix crack propagation is also modeled with VCCT. However, unlike delamination, the matrix crack is assumed to propagate following a Mode I path in the through-thickness direction, as supported by experimental evidence [8]. Therefore, the failure criterion is assumed to be given by:

$$f(G_T) = \frac{G_T}{G_{Ic}} - 1 = 0 \tag{21}$$

where G_{Ic} is assumed to be identical to the Mode I delamination fracture toughness, as demonstrated in [14]. At each crack growth increment, the Mode I crack path orientation is approximately determined using a maximum tangential stress criterion. This criterion, typically written in terms of the Mode I and II stress intensity factors [15], can also be written in terms of energy release rates G_I and G_{II},

where the angle θ that maximizes the tangential stress $\sigma_{\theta\theta}$ is obtained by evaluating:

$$\theta = 2\tan^{-1}\left(\frac{1}{4}\left[\left(\frac{G_I}{G_{II}}\right) \pm \sqrt{\left(\frac{G_I}{G_{II}}\right)^2 + 8}\right]\right) \tag{22}$$

and for the two solutions obtained choosing the one that maximizes $\widetilde{\sigma_{\theta\theta}}$ given by:

$$\begin{aligned}\widetilde{\sigma_{\theta\theta}} = \sqrt{G_I}\left\{3\cos\left(\frac{\theta}{2}\right) + \cos\left(\frac{3\theta}{2}\right)\right\} + \\ \sqrt{G_{II}}\mathrm{Sgn}(F_t)\left\{-3\sin\left(\frac{\theta}{2}\right) - 3\sin\left(\frac{3\theta}{2}\right)\right\}\end{aligned} \tag{23}$$

where F_t is the tangential component of the internal force vector **F** at the crack tip. The tangential stress $\sigma_{\theta\theta}$ relates to $\widetilde{\sigma_{\theta\theta}}$ by:

$$\sigma_{\theta\theta} = \frac{1}{4}\sqrt{\frac{E^*}{2\pi r}}\widetilde{\sigma_{\theta\theta}} \tag{24}$$

where,

$$E^* = \begin{cases} E & \text{plane stress} \\ \dfrac{E}{1-\nu^2} & \text{plane strain} \end{cases} \tag{25}$$

E is the Young's modulus; and ν the Poisson's ratio. Once the angle is determined, the criterion given by Equation 21 is assessed. If the criterion is met, the crack advances by one element along the projected crack path.

Fatigue

Matrix cracks are assumed to follow a Mode I path in the through-thickness direction, also in fatigue. In this case, the growth rate is simply obtained by:

$$\frac{\mathrm{d}a}{\mathrm{d}N} = A_I(G_{max})^{n_I} \tag{26}$$

and used to determine crack propagation in the fatigue algorithm implemented, which is discussed in a subsequent section. The growth rate of a matrix crack under Mode I loading is assumed to be well approximated by the growth rate of a delamination growing under the same loading conditions. This approach represents an extrapolation of the observations made in [14] for quasi-static loading conditions to the fatigue regime, and requires further experimental validation. Similar to Equation 18, Equation 26 does not account for R-ratio or frequency effects, and therefore its use is currently only recommended for R-ratios and frequencies that correspond to those used to generate the delamination fatigue characterization data.

MIGRATION

Criterion for delamination to matrix crack migration

STATIC

In the present work, the criterion for delamination migration proposed in [7] will be used. In this criterion, all variables needed to determine whether migration occurs, can be directly obtained from the FNM results at each interface crack position. Delamination migration is observed to be preceded by the creation of local micro cracks, oriented as a function of the principal stresses ahead of the crack tip, as discussed in [16]. If energetically favorable, these micro cracks can accumulate, propagating through one of the bounding plies (matrix crack), rather than accumulating and propagating along (or near) the interface (delamination), and migration is obtained [8]. The criterion proposed in [7] uses the sign of the tangential component of the internal force vector F_t, associated with Mode II shear displacement, to determine the direction of the micro cracks and therefore the material into which the interface crack would tend to migrate. Additionally, it assumes that migration can only be completed if it is energetically favorable. The criterion is given by $M_s: \{G_{II}^{Int}, G_T^{Int}, F_t\} \rightarrow \{-1,0,1\}$ as:

$$M_s = \begin{cases} \dfrac{\mathrm{Sgn}\left(\dfrac{G_T^{Int}}{G_c^A} - \dfrac{G_T^{Int}}{G_c^{Int}}\right) + 1}{2} \mathrm{Sgn}(F_t), & \mathrm{Sgn}(F_t) < 0 \\ \dfrac{\mathrm{Sgn}\left(\dfrac{G_T^{Int}}{G_c^B} - \dfrac{G_T^{Int}}{G_c^{Int}}\right) + 1}{2} \mathrm{Sgn}(F_t), & \mathrm{Sgn}(F_t) \geq 0 \end{cases} \tag{27}$$

where $M_s = 0$ if the interface crack does not migrate, and $M_S = -1$ or $M_S = 1$ if the crack migrates into material A or B, respectively (see fig. 4). In the present form, Equation 27 assumes that the internal force vector is computed at the lower surface (Material B). If the internal force vector is computed at the upper surface (Material A), the signs of the inequalities in Equation 27 need to be reversed. Depending on the sign of F_t, the ratio between the energy release rate determined at the interface, and the critical energy release rate of Material A or B, $\frac{G_T^{Int}}{G_c^A}$ or $\frac{G_T^{Int}}{G_c^B}$, is compared to the ratio between the energy release rate determined at the interface and the critical energy release rate of the interface, $\frac{G_T^{Int}}{G_c^{Int}}$. If the ratio $\frac{G_T^{Int}}{G_c^A}$ or $\frac{G_T^{Int}}{G_c^B}$ is greater than $\frac{G_T^{Int}}{G_c^{Int}}$, the necessary condition for migration is met, and $M_S = -1$ or $M_S = 1$. Note that although this criterion is necessary, it is not sufficient for migration to occur unless the ratio being assessed is greater than one, i.e. the failure criterion for delamination or matrix cracking need to be met. Figure 4 illustrates how the migration criterion interplays with the failure criteria for delamination and matrix cracking, to determine whether delamination, migration or neither will occur. Figure 4 also shows the principal stress resultant for positive and negative applied shear, see fig. 4a and 4b, respectively.

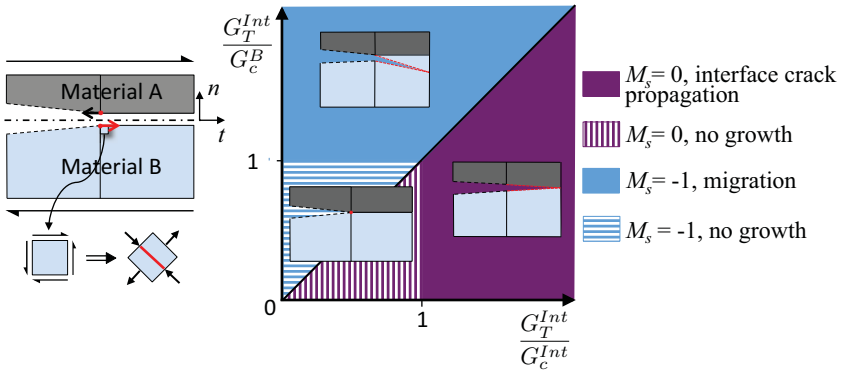

a) positive shear

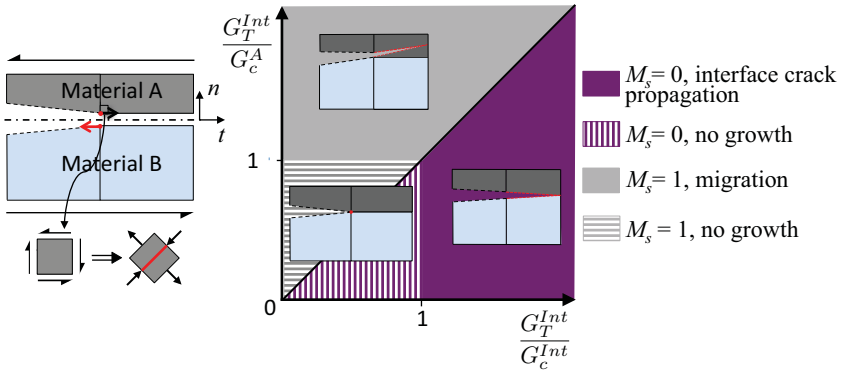

b) negative shear

Figure 4 Illustration of the combination between failure and migration criteria used to determine delamination migration, Equations 16 and 21, and Equation 27, respectively.

FATIGUE

The criterion used to predict migration under fatigue shares the same basic premises as the migration criterion used in the quasi-static case. The shear sign dictates the direction towards which the delamination will tend to migrate. To determine whether migration will occur, the fatigue crack growth rate in the material into which the delamination will tend to migrate is compared to the fatigue crack growth rate of the delamination. Similar to the static case, the criterion is given by $M_f: \{G_{II}^{Int}, G_T^{Int}, F_t\} \rightarrow \{-1,0,1\}$ as:

$$M_f = \begin{cases} \dfrac{\mathrm{Sgn}\left(\left(\dfrac{da}{dN}\right)_A - \left(\dfrac{da}{dN}\right)_{Int}\right)+1}{2}\mathrm{Sgn}(F_t), & \mathrm{Sgn}(F_t) < 0 \\ \dfrac{\mathrm{Sgn}\left(\left(\dfrac{da}{dN}\right)_B - \left(\dfrac{da}{dN}\right)_{Int}\right)+1}{2}\mathrm{Sgn}(F_t), & \mathrm{Sgn}(F_t) \geq 0 \end{cases} \tag{28}$$

If $M_f = 0$, the interface crack does not migrate, and if $M_f = -1$ or $M_f = 1$, the crack migrates into material A or B, respectively. The criterion is illustrated in Figure 5, for positive and negative shear sign applied. In the present work, the interfacial crack, or delamination, propagates between a 0° and a 90° ply. Assuming Material A is the 0° ply, and Material B is the 90° ply, the growth rate of

a crack growing into a 0° ply is considered to be much lower than the growth rate for a crack to propagate at the interface, since fiber fracture is required for that process to occur. Thus, $\left(\frac{\mathrm{d}a}{d\mathrm{N}}\right)_A$ is always much smaller than $\left(\frac{\mathrm{d}a}{d\mathrm{N}}\right)_{Int}$. Therefore, even if the sign of F_t favors migration into Material A (0° ply), according to Equation 28, migration will not occur. This criterion translates the hypothesis that, due to the difference in growth rates, the crack will advance along the interface before enough cycling has occurred for it to migrate towards Material A. In the present study, it is considered that the growth rate of a Mode I matrix crack can be characterized by Equation 26, while the delamination growth rate, $\left(\frac{\mathrm{d}a}{d\mathrm{N}}\right)_{Int}$, is assumed to be given by Equation 18. Since both are of the same order of magnitude, if the sign of F_t favours migration into Material B (90° ply) depending on the relative magnitude of $\left(\frac{\mathrm{d}a}{d\mathrm{N}}\right)_A$ and $\left(\frac{\mathrm{d}a}{d\mathrm{N}}\right)_{Int}$, migration can occur.

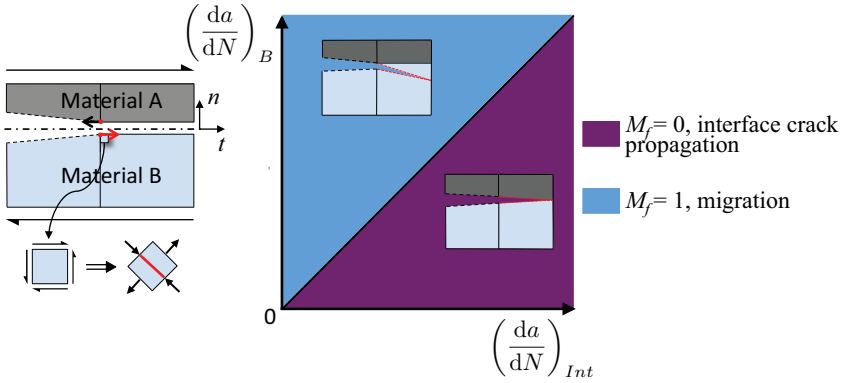

a) positive shear

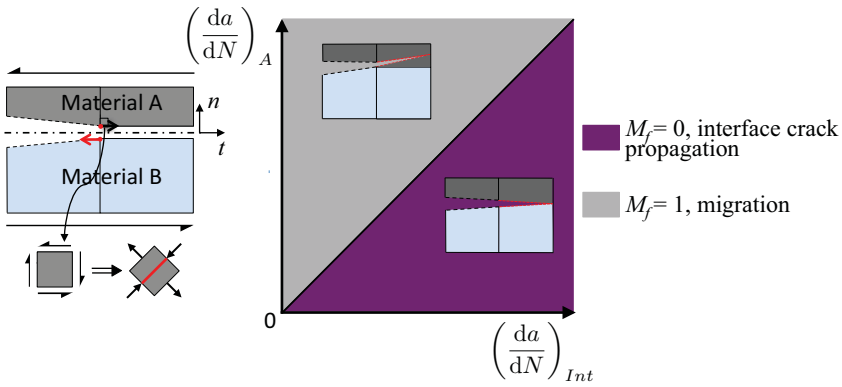

b) negative shear

Figure 5 Illustration of the fatigue migration criterion, Equation 28.

Matrix crack to delamination transition

When a matrix crack reaches a weak interface, it is assumed to trigger delamination, both under static and fatigue loading conditions. This delamination is at first contained within the FNM element, as illustrated in fig. 2(f). In the following steps, the delamination will propagate, or migrate, as detailed in the previous sections.

FATIGUE ALGORITHM

The algorithm used to propagate fatigue cracks in the present work is illustrated in fig. 6, and is described next.

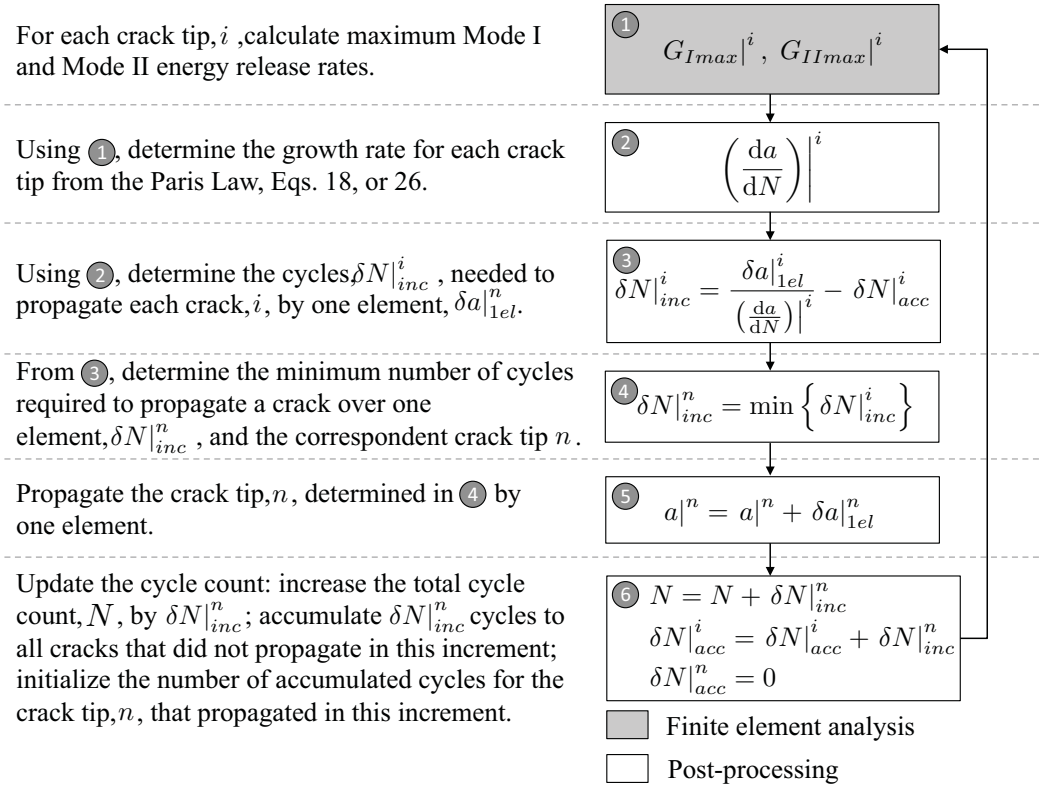

Figure 6 Fatigue algorithm implemented.

In the first step, $G_{Imax}|^i$ and $G_{IImax}|^i$ are determined for each crack tip, i. In the present work, only the maximum energy release rate is used to obtain delamination and matrix crack growth rate, Equations 18, and 26. Often Paris Law equations, accounting for R-ratio and frequency effects, require the calculation of both G_{Imin} and G_{IImin}, or ΔG. In the context of the present algorithm, G_{Imin}, G_{IImin} could be obtained through an additional finite element analysis per increment. Having determined $G_{Imax}|^i$ and $G_{IImax}|^i$, the number of cycles, $\delta N|^i_{inc}$, that are needed to propagate each crack i by the length correspondent to the next element are obtained from:

$$\delta N|^i_{inc} = \frac{\delta a|^i_{1el}}{\left(\frac{\mathrm{d}a}{\mathrm{d}N}\right)\Big|^i} - \delta N|^i_{acc} \tag{29}$$

where $\delta a|^i_{1el}$ is the length of the element ahead of the crack i, and $\delta N|^i_{acc}$ is the number of cycles accumulated by the crack tip before it grows to the next element. Subsequently, the minimum number of $\delta N|^i_{inc}$ and the correspondent crack tip are determined, $\delta N|^n_{inc}$ and n, respectively. This determines the cycle increment in this

iteration. The crack tip n is advanced by the correspondent $\delta a|_{1el}^{n}$. The accumulated cycle count of all crack tips (except n) as well as the total cycle count, are incremented by $\delta N|_{inc}^{n}$. Finally, the accumulated cycle count for the crack tip n is set to zero, and a new increment starts.

SIMULATION OF DELAMINATION MIGRATION SPECIMENS

Delamination migration test configuration

In reference [8], a test aimed at investigating delamination migration was proposed. The Delamination Migration (DM) test configuration is illustrated in fig. 7. The specimen has three key features that enable the controlled observation of delamination growth followed by migration to another ply interface. First, the specimen geometry is in the form of a beam with the intent of promoting uniform delamination growth and migration across the specimen width. Second, the specimen contains a Teflon insert (acting as an artificial delamination) at an interface between a 0° ply (specimen span direction) and a stack of four 90° plies (specimen width direction) (fig. 7). This provides an opportunity for the delamination to migrate to another ply interface by kinking through the 90° ply stack. Third, the specimen can be loaded in a manner to cause delamination growth from the Teflon insert that eventually migrates to another ply interface. This sequence of fracture events is made possible by the way in which specimen loading affects shear stresses acting across the delamination front.

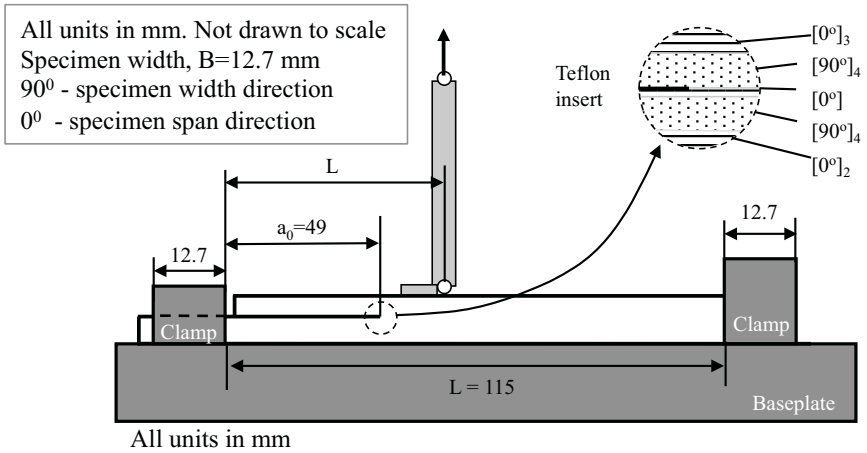

Figure 7 Delamination Migration (DM) test configuration [8].

Finite Element Model

The simulations presented in this work were all performed using the finite element solver Abaqus/Standard® 6.13 (Implicit). Plane-strain and a small-displacement formulation were used. The floating node element (fig. 2) was developed and implemented as a user defined element (UEL) in Abaqus/Standard®, and applied in the center region of the model, as shown in fig. 8. The specimen layup used in the experiments and in the model, is also given in fig. 8. In the layup description 'T' represents the Teflon insert. Each block of plies of the same orientation was modeled with a separate element CPE4 (through-thickness), except for the highlighted plies at the center of the model (fig. 8). These plies were modeled

within a single FNM element, as illustrated in fig. 2. Rigid contact with friction is assumed between the bottom surface of the specimen and the baseplate, and the top surface of the specimen and the clamps. All the material properties used, including the friction coefficient, are given in Tables I, II and III. A displacement was applied at a single node, at different load offsets L, to simulate a displacement-controlled test, see fig. 8. All tests were performed under ambient laboratory conditions.

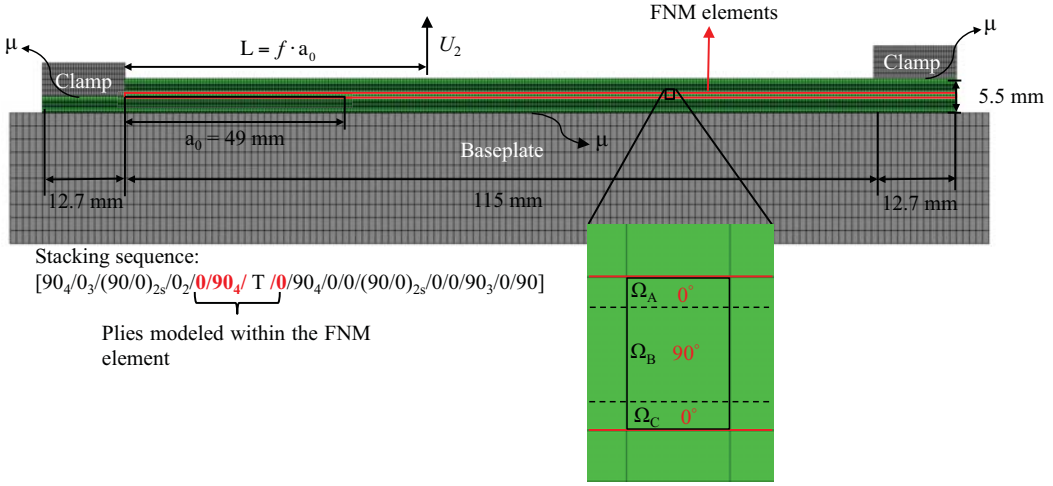

Figure 8 Finite element model used.

TABLE I. ELASTIC PROPERTIES, IM7-8552 [17]

E_{11}	$E_{22} = E_{33}$	$\nu_{12} = \nu_{13}$	ν_{23}	$G_{12} = G_{13}$	G_{23}
161.0 (GPa)	11.38 (GPa)	0.32	0.44	5.17(GPa)	3.98(GPa)

TABLE II. FRICTION COEFFICIENT CARBON/EPOXY TO ALUMINUM [18] AND CRITICAL ENERGY RELEASE RATES FOR DELAMINATION OF IM7-8552 [19].

μ	G_{Ic}	G_{IIc}	η
0.23	0.21 (kJ/m^2)	0.77(kJ/m^2)	2.1

TABLE III. PARIS LAW COEFFICIENTS FOR MODE I AND MODE II OF IM7-8552 [11,12].

A_I	n_I	A_{II}	n_{II}
8.757E-6	6.71	6.84E-7	5.45

BOUNDARY CONDITIONS

As illustrated in fig. 7, the DM specimen is clamped at both ends. Each clamp was tightened using three screws at a fixed applied torque. The clamping conditions were simulated in a first step, by applying the clamping force, estimated to be 1700 N, via two reference nodes coupled to the top surface of each clamp through a displacement constraint. Finally, and as was mentioned previously, rigid contact with friction was used to model the interaction between clamps, specimen and baseplate. To assess the adequacy of the boundary conditions applied, the deflection of a DM specimen was measured using Digital Image Correlation (DIC) and compared to the numerical results. Figure 9 compares the DIC results with deflections obtained from three different numerical models. The curve labeled 'FIXED', was obtained using a numerical model with nominal dimensions, and

where the clamping conditions were idealized by fixing the displacement at the top and bottom surfaces of the specimen in the clamped region. It is evident that this model under-predicts the deflection. Furthermore, the maximum load is also not aligned with the maximum deflection observed experimentally. Measuring the exact load-application point and crack-tip position of the specimen tested, it was observed that both deviated from the nominal values. Including this correction in the model the curve 'FIXED-CORR' was obtained. The maximum deflection in this curve is now aligned with the observed experimentally, but the magnitude is still underestimated. Finally, the third curve, 'CLAMP', is obtained by applying the clamping force to the model in an initial step (including the corrected crack length and load-application point), and modeling the contact between clamps, specimen and baseplate, as described above. It is evident that these boundary conditions lead to the best agreement with the experimental data. However, the deflection seems slightly overestimated, near the left-hand-side clamp, which could be caused by an underestimation of the local clamping force, or friction coefficient.

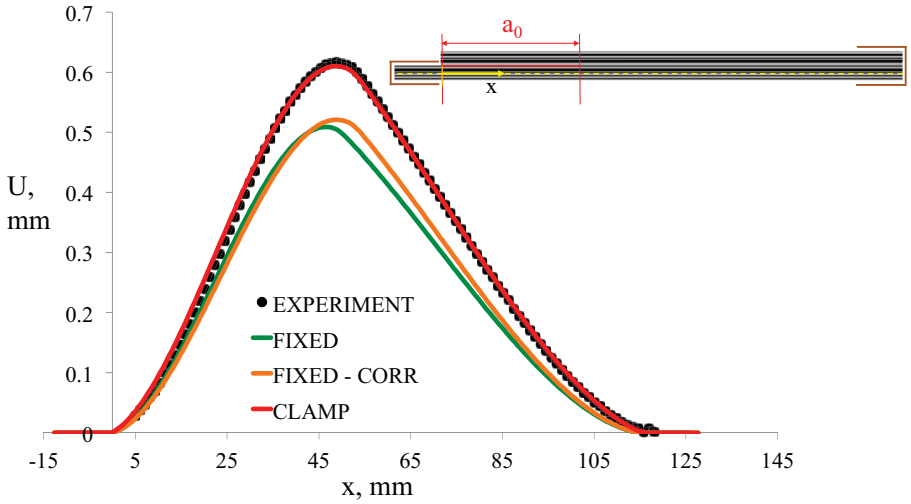

Figure 9 Comparison between a specimen deflection measured using DIC and the simulations.

Results

QUASI-STATIC LOADING

Overall, the framework proposed is capable of predicting and simulating delamination migration in cross-ply laminates under quasi-static conditions. Fig. 10 compares the computed load-displacement curves obtained, for two values of L, with experiments illustrating the accuracy of the approach. Overall, the maximum load is well predicted for both cases. For $L = a_0$, the simulations predict unstable delamination after the peak load (fig. 10(a)). This unstable delamination stops just before migration. After the migration event, delamination arrests, and upon further loading it continues propagating stably along the next $0°/90°$ interface. A similar sequence of events was observed experimentally [7]. However, in the experiments, after the first unstable event, further loading was necessary before migration occurred. For the case $L = 1.3a_0$, the simulations predict that the first peak in load is followed by a region of stable delamination growth. A region of unstable

delamination, corresponding to the load-drop follows as shown in fig. 10(b). The migration event is predicted to occur in this region. After the migration, unstable delamination continues propagating along the next $0°/90°$ interface. Loading the specimen further eventually leads to a transition from unstable to stable delamination propagation. This sequence of events is identical to what was reported experimentally [8]. The only difference observed is that in the experiments, after the peak load, delamination propagates through a series of unstable events, rather than stably, as predicted by the simulations. Further simulations for other load-offsets, namely $L = 1.1a_0$ and $L = 1.2a_0$ were performed and compared to the experimental results, showing a similar agreement.

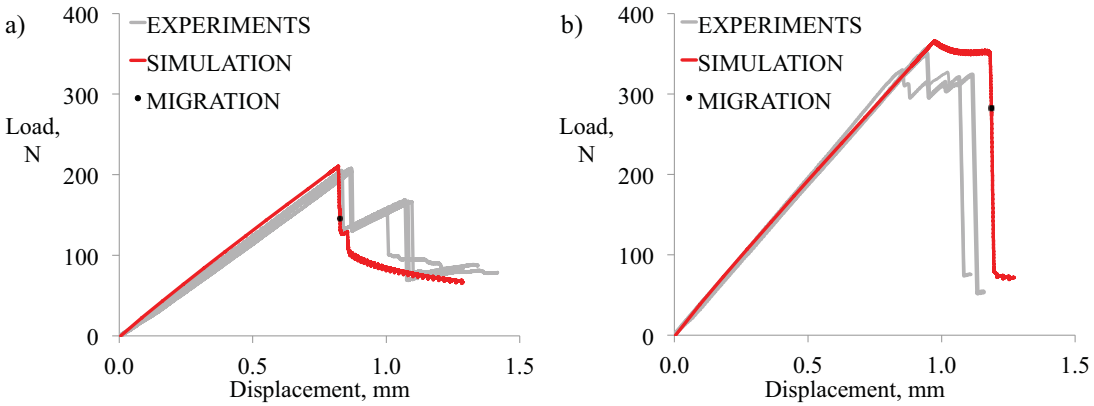

Figure 10 Load displacement curves for (a) load-offset L=a_0 and (b) L=1.3a_0

FATIGUE LOADING

Constant amplitude fatigue conditions were simulated. A maximum displacement corresponding to $G_{Tmax} = 0.8G_c$ was applied, where G_c was determined from the quasi-static simulations. This G_c corresponds to the critical energy release rate to initiate delamination for each load-offset L. The frequency of the fatigue loading was assumed to be 5Hz, and the ratio of minimum to maximum displacement, R-ratio, $\frac{(U_2)_{min}}{(U_2)_{max}} = 0.1$. Both R-ratio and frequency are the same used to obtain the fatigue characterization data summarized in Table III.

Overall the predicted damage morphology was similar in both quasi-static loading and fatigue, only fatigue results are shown here for brevity. Figure 11(a) provides an illustration of a typical crack path predicted by the simulations. Figure 11(b) shows the distance from the load-application point to migration, Δ_K, as a function of the normalized load offset, L/a_0. The simulations predict a decreasing trend in Δ_K with L/a_0, which is similar to what was observed in the static case [8].

Figure 12(a) shows two curves corresponding to the number of cycles to migration onset and to $\delta a = 3$ mm past the completed migration as a function of the load-offset, labeled 'MIGRATION - INI', and 'MIGRATION + δa', respectively. Comparing 'MIGRATION - INI' to 'MIGRATION + δa', it is clear that they only differ noticeably for $L = a_0$. Overall, simulations predict a significant increase in cycle count to migration as the load-offset increases. This trend can be further examined by analyzing the crack growth as a function of number of cycles. Figure 12(b) presents delamination growth up to migration for two different load-offsets

$L = a_0$ and $L = 1.3a_0$. Comparing the results obtained for the two offsets, it is possible to see that for $L = 1.3a_0$ a significant decrease in crack growth rate can be observed, between N=50000 and N=150000, before it increases again leading to further delamination and migration.

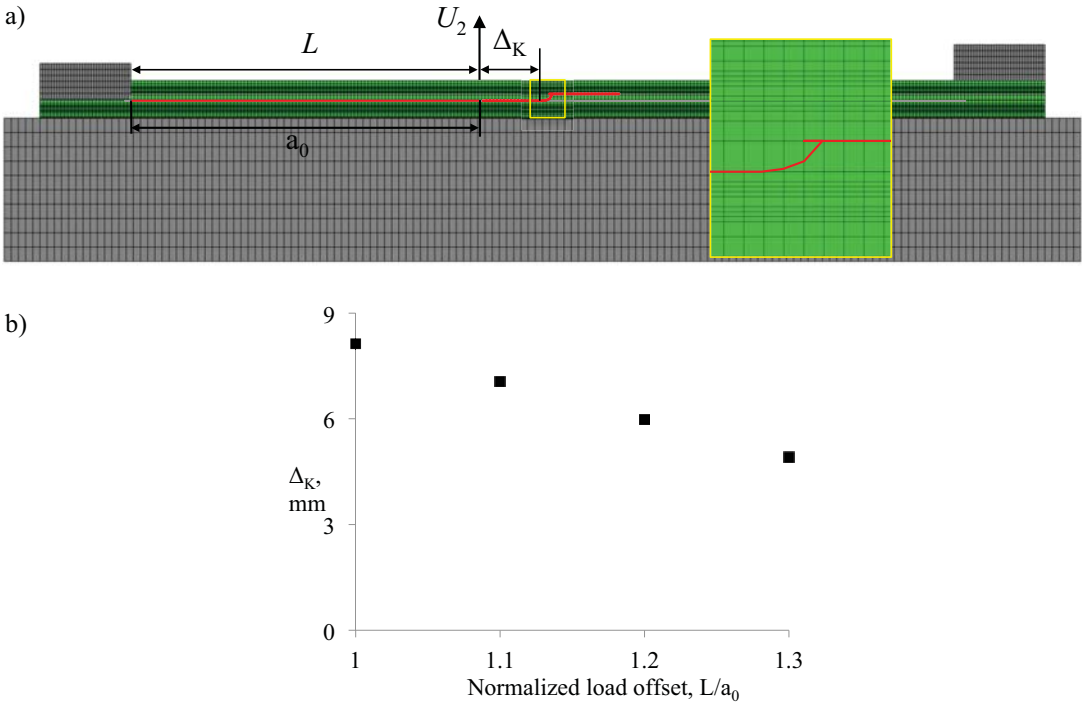

Figure 11(a) typical crack path, (b) distance from the migration location to the load-application point, Δ_K, as a function of load-offset L.

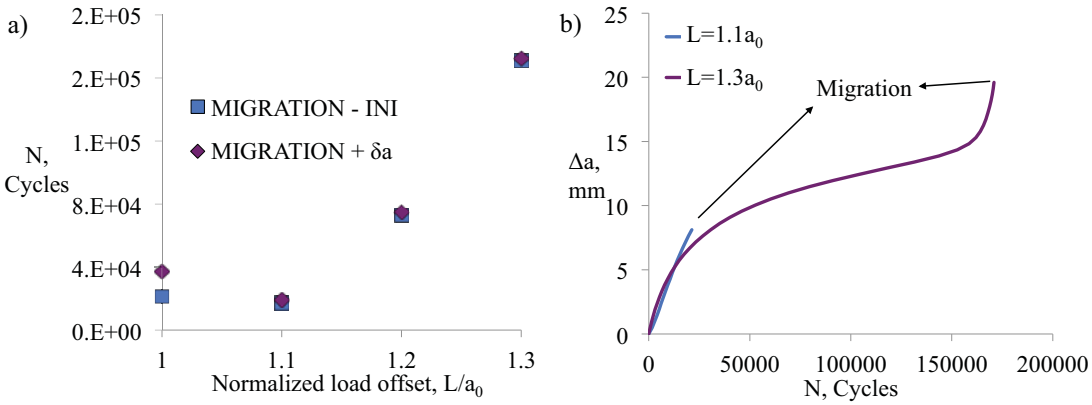

Figure 12 (a) number of cycles to migration onset, and to migration onset + $\delta a = 3$ mm, and (b) delamination growth prior to migration as a function of number of cycles.

DISCUSSION

The detailed analysis of the specimen deflection using DIC has helped in assessing the adequacy of the boundary conditions applied. Nevertheless, the clamping force and friction coefficient are likely to vary slightly from specimen to specimen.

Therefore, further sensitivity studies are recommended to characterize fully the effect of the boundary conditions on the overall response of the specimens.
Overall, the sequence of events, failure morphology and load-displacement curves are in good agreement with the experimental results. However, for the case $L = a_0$, experimental results show an increase in load at the end of the first unstable event, before migration, not predicted by the simulations. Also, for $L = 1.3a_0$, the simulations predict stable delamination, prior to the final load-drop, while experiments show that the delamination propagates through a series of unstable events. One of the main differences between simulations and experiments, is the assumption that the delamination propagates at the interface between the 0° and 90° ply. However, in the experiments, it is often observed that delamination delves slightly into 0° ply propagating just within it, and leads to the development of bridging fibers. This mechanisms is thought to be caused by the applied shear force that tends to drive the delamination into the 0° ply in the first part of the test (for the load offsets tested). Delamination delving, and the associated fiber bridging, leads to local variations in G_c not accounted for by the model, and likely to lead to some of the discrepancies observed.
The predicted damage morphology under fatigue loading conditions is similar to the one obtained under quasi-static loading, including migration location [8]. Overall, simulations predict an increase in cycles to migration as a function of the load-offset. For the $L = 1.3a_0$ case the delamination growth rate decreases substantially before it increases again and migration occurs. This decrease indicates that for lower displacements applied, a fatigue threshold may be reached, before migration is obtained. Further, also the delamination delving mechanism observed in the static tests might occur in fatigue, since it is a function primarily of the shear sign applied. The delving may alter (decrease) the growth rates obtained in the characterization tests. Hence, threshold values might be reached even for high-applied loads, and overall the results obtained with the present approach, may be overly conservative, i.e. more crack growth is predicted for the same number of applied cycles. In the present work, the fatigue loading simulated was chosen to be consistent with the characterization data available, i.e. same R-ratio, and frequency. A more general fatigue loading scenario would require either further characterization data, or the use of a modified Paris Law that can potentially account for these effects [20]. Furthermore, the first order approximation used to determine the variation of delamination growth rate with mode-mixity, Equations 19 and 20, can potentially be improved given the recent experimental data obtained [13]. Finally, although the fatigue algorithm and overall approach has been demonstrated, experimental validation is needed.

CONCLUSIONS

The FNM (Floating Node Method) was combined with VCCT (Virtual Crack Closure Technique) and used to model delamination migration in cross-ply laminates under quasi-static and fatigue loading conditions. Delamination, matrix cracking, and migration, are all modeled with the same FNM element using failure and migration criteria based on fracture mechanics. As a result, the present approach only uses material properties, the majority of which can be obtained using

well established standard characterization tests. For quasi-static loading, the results obtained compared favorably with experimental results available. Regarding fatigue, the algorithm and migration criterion have been demonstrated. However, experimental validation is still required.

REFERENCES

[1] Ling, D., Q. Yang, B. Cox. 2009. "An augmented finite element method for modeling arbitrary discontinuities in composite materials," *International Journal of Fracture*, 156(1):53-73.

[2] Iarve, E.V., M.R. Gurvich, D.H. Mollenhauer, C.A. Rose and C.G. Dávila. 2011. "Mesh-independent matrix cracking and delamination modeling in laminated composites," *Int. J. Numer. Meth. Engng.*, 88(8):749-773.

[3] van der Meer, F.P., L.J. Sluys, S.R. Hallet and M.R. Wisnom. 2012. "Computational modeling of complex failure mechanisms in laminates," *Journal of Composite Materials*, 46(5):603-623.

[4] Chen, B.Y., S.T. Pinho, N.V. De Carvalho, P.M. Baiz, and T.E. Tay. 2013. "Floating node method for the modeling of multiple discontinuities within an element," *19th International conference on Composite Materials*, Montreal.

[5] Rybicki, E.F., M.F. Kannine. 1977. "A finite element calculation of stress intensity factors by a modified crack closure integral," *Eng. Fract. Mech.*, 9:931-938.

[6] R. Krueger. 2004. "Virtual crack closure technique: history, approach and applications," *Applied Mechanics Reviews,* 57:109-143.

[7] De Carvalho, N.V., B.Y. Chen, S.T. Pinho, P.M. Baiz, J.G. Ratcliffe, T.E. Tay. 2013. "Floating node method and virtual crack closure technique for modeling matrix cracking-delamination interaction," NASA/CR-2013-218022.

[8] Ratcliffe, J.G., M.W. Czabaj, T.K. O'Brien. 2012. "Characterizing delamination migration in carbon/epoxy tape laminates," *Proceedings of the American Society for Composites – Twenty-Seventh Technical Conference*, Arlington, TX, USA, paper 313.

[9] Benzeggagh, M.L., M. Kenane. 1996. "Measuring of mixed-mode delamination fracture toughness of unidirectional glass/epoxy composites with mixed-mode bending apparatus," *Composites Science and Technology*, Vol. 56:439-449.

[10] Blanco, N., E.K. Gamstedt, L.E. Asp, J. Costa. 2004. "Mixed-mode delamination growth in carbon–fibre composite laminates under cyclic loading." *International journal of solids and structures* 41(15):4219-4235.

[11] Murri, G.B. 2013. "Evaluation of delamination onset and growth characterization methods under mode I fatigue loading," NASA/TM-2013-217966.

[12] O'Brien, T. K., W. M. Johnston, J. T. Gregory. 2010. "Mode II interlaminar fracture toughness and fatigue characterization of a graphite epoxy composite material," NASA/TM–2010-216838.

[13] Ratcliffe, J.G., W. M. Johnston 2014. "Influence of mixed mode I-mode II loading on fatigue delamination growth characteristics of a graphite epoxy tape laminate," *Proceedings of the American Society for Composites – 28th Technical Conference*, San Diego, CA, USA, paper 663.

[14] Czabaj, M.W., J.G. Ratcliffe. 2012. "Comparison of intralaminar and interlaminar mode-I fracture toughness of unidirectional IM7/8552 graphite/epoxy composite," *Proceedings of the American Society for Composites – 27th Technical Conference*, Arlington, TX, USA, paper 114.

[15] Moës, N., J. Dolbow, T. Belytschko. 1999. "A finite element method for crack growth without remeshing," *Int. J. Numer. Meth. Engng.* 46:131-150.

[16] Greenhalgh, E.S., C. Rogers, P. Robinson. 2009. "Fractographic observations on delamination growth and the subsequent migration through the laminate." *Composites Science and Technology*, 69:2345-2351.

[17] O'Brien, T. K., R. Krueger. 2003. “Analysis of flexure tests for transverse tensile strength characterization of unidirectional composites,” *Journal of Composites Technology and Research,* 25:50-68.

[18] Schön, J. 2004. “Coefficient of friction for aluminum in contact with a carbon fiber epoxy composite.” *Tribology International* 37(5): 395-404.

[19] Krueger, R. 2012. “Development and application of benchmark examples for mixed-mode I/II quasi-static delamination propagation predictions,” NASA/CR-2012-217562.

[20] Allegri, G., M. R. Wisnom, and S. R. Hallett. 2013. “A new semi-empirical law for variable stress-ratio and mixed-mode fatigue delamination growth.” *Composites Part A: Applied Science and Manufacturing* 48:192-200.